phys. stat. sol. (a) **205**, No. 4, 901–904 (2008) / **DOI** 10.1002/pssa.200777892

physica status solidi a
www.pss-a.com
applications and materials science

# Real time spectroscopic ellipsometry of sputtered CdTe, CdS, and $CdTe_{1-x}S_x$ thin films for photovoltaic applications

**Jian Li[1], N. J. Podraza[1,2], and R. W. Collins[*,1]**

[1] Department of Physics and Astronomy, The University of Toledo, Toledo, OH 43606, USA
[2] Materials Research Institute, The Pennsylvania State University, University Park, PA 16802, USA

Received 31 July 2007, accepted 16 December 2007
Published online 26 March 2008

**PACS** 07.60.Fs, 73.40.Lq, 78.20.Ci, 78.66.Hf, 84.60.Jt

[*] Corresponding author: e-mail robert.collins@utoledo.edu, Phone: +001 (419) 530-2195, Fax: +001 (419) 530-2723

Real time spectroscopic ellipsometry (RTSE) has been applied to study the deposition of polycrystalline CdTe, CdS, and $CdTe_{1-x}S_x$ thin films on crystalline silicon wafer substrates as well as the formation of CdS/CdTe and CdTe/CdS heterojunctions, all using a magnetron sputtering process. For CdTe and CdS, the key process variable is deposition temperature ($T$). The nucleation and growth behaviors of CdTe and CdS show strong variations with $T$ and this influences the ultimate grain size of the polycrystalline films. For the co-sputtered $CdTe_{1-x}S_x$ alloys, the key variables are the rf power levels applied to the CdTe and CdS targets and thus the resulting composition $x$. The dielectric functions of the alloys have been used as a database for real time investigation of inter-diffusion at the CdS/CdTe and CdTe/CdS heterojunctions.



**1 Introduction** Magnetron sputtering is of great interest for the deposition of thin film CdTe, CdS, and related alloys, as this technology has been used for 14%-efficient polycrystalline CdS/CdTe heterojunction solar cells, with an advantage of low processing temperatures [1]. *In situ*, real time analyses of photovoltaic thin films are important owing to the insights they provide into the structural evolution of the films and its influence on the ultimate film properties, as well as into heterojunction formation. Such insights can be used to control multi-step processing and to optimize interface, bulk, and surface properties separately for high performance cells. Real time spectroscopic ellipsometry (RTSE) is a powerful technique which has been used successfully for optimization of a-Si:H solar cells prepared by plasma-enhanced chemical vapor deposition [2] and is more recently being used for optimization of sputter deposition and $CdCl_2$ post-processing of CdS/CdTe solar cells [3].

**2 Experimental details** Polycrystalline CdTe, CdS, and $CdTe_{1-x}S_x$ films were magnetron sputtered under the conditions listed in Table 1, which are similar to those yielding 14%-efficient solar cells [1]. Native oxide-covered crystalline Si wafers were used as substrates due to their consistent smoothness. The deposition temperature $T$, a key process variable, was determined from the $E_0$ band gap shifts that occur upon cooling the deposited film to 15 °C and reheating to the deposition temperature $T$ [3]. $CdTe_{1-x}S_x$ alloys were deposited at $T = 190$ °C, which is close to the highest temperature possible without phase segregation [4]. The design principles of the rotating compensator multichannel ellipsometer used in this study are analogous to those developed to study a-Si:H based solar cells [5].

The instrument provides ellipsometric spectra ($\psi$, $\Delta$) over the spectral range of 0.75 eV to 6.5 eV. In this study, the spectra were acquired in times from 1 s to 3 s, as averages over ~30 to 90 optical cycle pairs, during which ≤3 Å deposited material has accumulated.

## 3 Results and discussion

**3.1 Nucleation and growth mode** In analyses of RTSE data in the initial stages of the deposition, a model for the film was used consisting of two layers, (i) a dense layer of thickness $d_b$ with a bulk-like dielectric function and (ii) a surface roughness layer of thickness $d_s$ with a di-

**Table 1** CdTe, CdS, and $CdTe_{1-x}S_x$ deposition parameters.

| deposited material | RF power (Watt) | Ar pressure (mTorr) | Ar flow (sccm) | deposition temperature (°C) |
|---|---|---|---|---|
| CdTe | 60 | 18 | 23 | 188–304 |
| CdS | 50 | 10 | 23 | 145–320 |
| $CdTe_{1-x}S_x$ | co-sputtering CdTe: 20–75 CdS: 33–53 | 18 | 23 | 190 |

electric function determined from the Bruggeman effective medium theory as a 0.5/0.5 volume fraction mixture of (bulk material)/void [6]. Figure 1 shows the time evolution of $d_b$ and $d_s$ for CdS deposition at three temperatures. At $T = 145$ °C, a ~6 Å thick roughness layer appears before the first dense monolayer (ML) (~3 Å), as shown in Fig. 1(a). This is typical of the island or Volmer–Weber (V–W) nucleation mode [7]. At $T = 225$ °C, ~1–2 dense MLs appear before the first ML of roughness, as shown in Fig. 1(c). This is typical of the layer-to-island or Stranski–Krastanov (S–K) growth mode [7]. At $T = 160$ °C, the first MLs of surface roughness and dense material appear virtually simultaneously, as shown in Fig. 1(b). This temperature describes a transition from V–W to S–K modes. At higher $T$, a layer-by-layer mode is favored for both CdTe and CdS [8] due to a reduction in free energy density of the interface relative to that of the surface, possibly as a result of enhanced diffusion at higher $T$ [7]. Figure 2(a) shows that the V–W to S–K transition temperature (vertical lines) is ~160 °C for CdS and ~260 °C for CdTe, indicating a lower diffusion activation energy for CdS. The peak nuclei height for CdTe is larger than that for CdS as observed in Fig. 2(b), indicating a lower nuclei density in the initial stages. In both cases, the nucleation density decreases with increasing deposition temperature.

Different nucleation behavior in the initial stage of deposition has been observed to impact the subsequent structural evolution of film and ultimate material properties, as has been discussed previously [8].

**3.2 Grain size effects** Each CdS film was sputtered to a thickness of $d_b \sim 500$ Å with $T$ in the range of 145–320 °C and then cooled under vacuum and measured by SE to obtain its room temperature complex dielectric function $\varepsilon$, as shown in Fig. 3. The $E_0$ (fundamental gap), $E_1$-$A$, and $E_1$-$B$ critical points (CPs) are evident [9]. To quantify the CPs, the second derivative spectra in $\varepsilon$ were fit assuming the standard lineshape:

$$\varepsilon = \sum_n A_n (E - E_n - i\Gamma_n)^{\mu_n} \exp(i\phi_n), \quad (1)$$

where $A_n$, $E_n$, $\Gamma_n$, $\mu_n$, and $\phi_n$ are the amplitude, band gap, broadening parameter, exponent, and phase of the $n$-th CP, respectively [10]. The best fit broadening parameter $\Gamma_n$ is plotted as a function of deposition temperature in Fig. 4.

The CP features of the sample deposited at 310 °C with the smallest $\Gamma_n$ (circled in Fig. 4) are even sharper than those of single crystal hexagonal CdS, as measured in this study as well as by Ninomiya et al. [9]. Thus, $\Gamma_n$ for this sample can be taken as intrinsic to single crystal CdS (denoted by $\Gamma_{bn}$), and can be related to the band structure of CdS. Assuming the parabolic band approximation for the $E_0$ transition with electron and hole effective masses of $m_e^* = 0.2m_e$ and $m_h^* = 0.7m_e$ [11], the group speed associated with this excitation can be estimated as $v_{g0} \sim 2.2 \times 10^5$ m/s. If the dominant broadening effect is taken to be a result of the limited excitation lifetime due to grain boundary scattering, then the following relation can be applied:

$$\Gamma_n = \Gamma_{bn} + hv_{gn}/R, \quad (2)$$

where $R$ is the deduced grain radius [12]. Using the values of $v_{g0}$ and $\Gamma_{b0}$ for single crystal CdS, $R$ can be calculated as a function of $T$ as shown in Fig. 5. As a check of the correctness of the general approach, the other two critical point widths $\Gamma_{E_1\text{-}A}$ and $\Gamma_{E_1\text{-}B}$ are plotted versus $R^{-1}$ in Fig. 6. Equation (2) is closely followed with group speeds for the $E_1$-$A$ and $E_1$-$B$ excitations of $3.3 \times 10^5$ and $8.8 \times 10^5$ m/s.

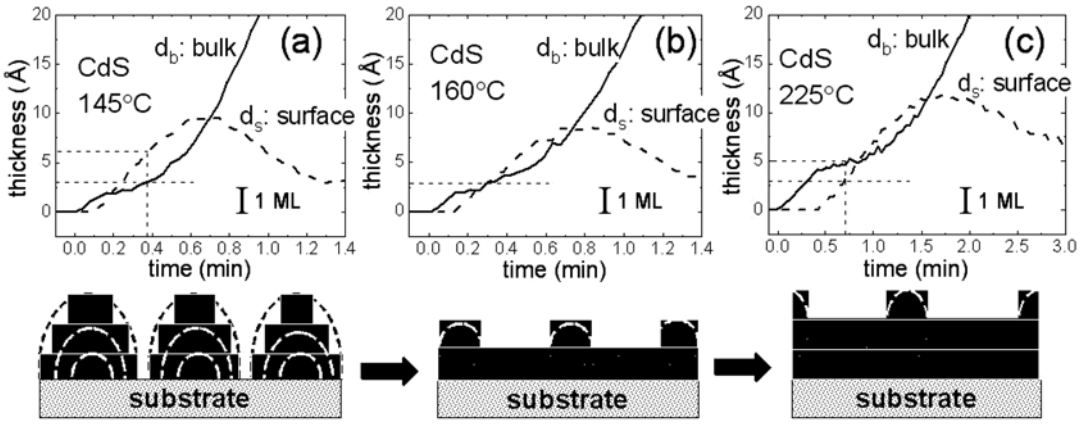


**Figure 1** Nucleation modes of CdS thin films deposited at different temperatures: (a) 145 °C; (b) 160 °C; (c) 225 °C.

 

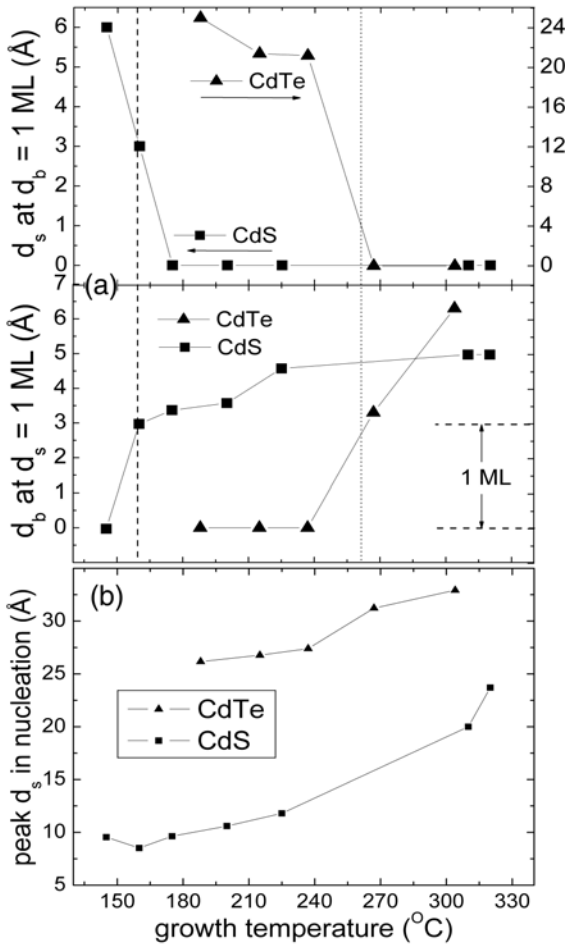


**Figure 2** (a: top two panels) Key nucleation parameters: $d_s$ when the first complete dense ML appears (upper panel); $d_b$ when the first surface roughness monolayer forms (center panel); peak nucleation height before coalescence (b: lower panel).

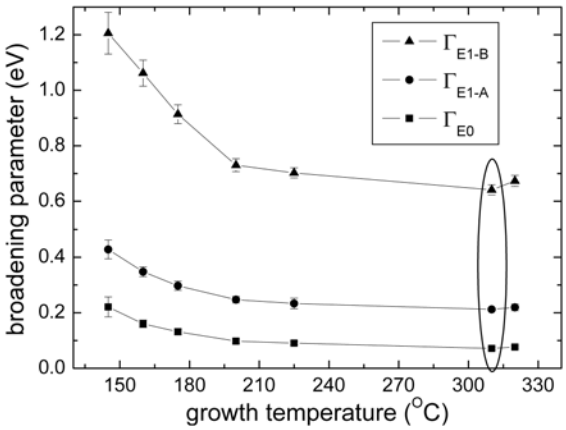


**Figure 4** Broadening parameter measured at ~15 °C for CdS films deposited at different $T$; the lowest values are circled.

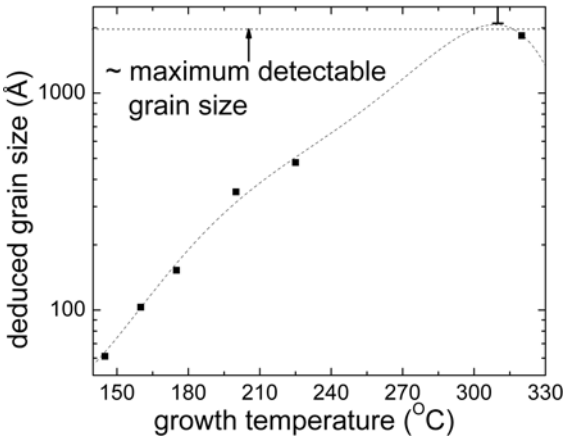


**Figure 5** Grain radius $R$ estimated from the broadening parameter of the $E_0$ transition by using the inverted form of Eq. (2).

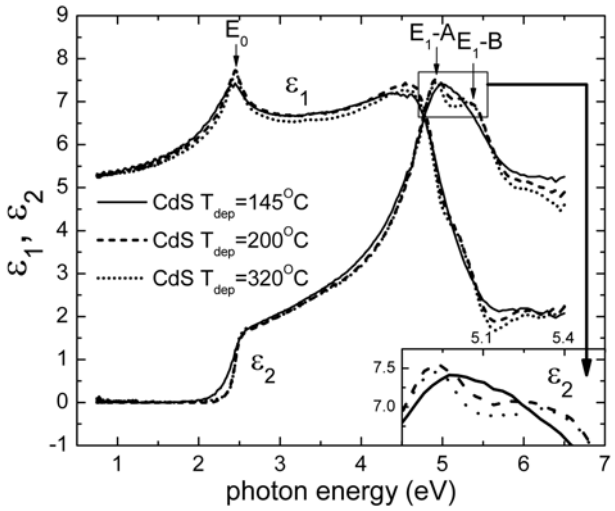


**Figure 3** Dielectric functions measured at ~15 °C for CdS films magnetron sputter-deposited at different temperatures.

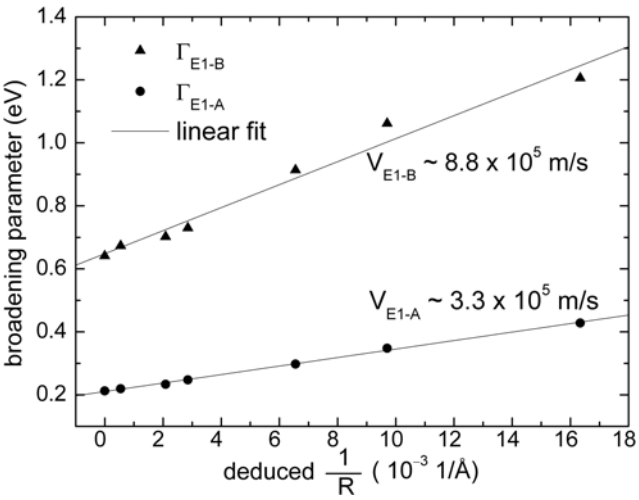


**Figure 6** Broadening parameters of the $E_1$-$A$ and $E_1$-$B$ CPs vs. inverse grain size; group speeds from the linear fits are indicated.

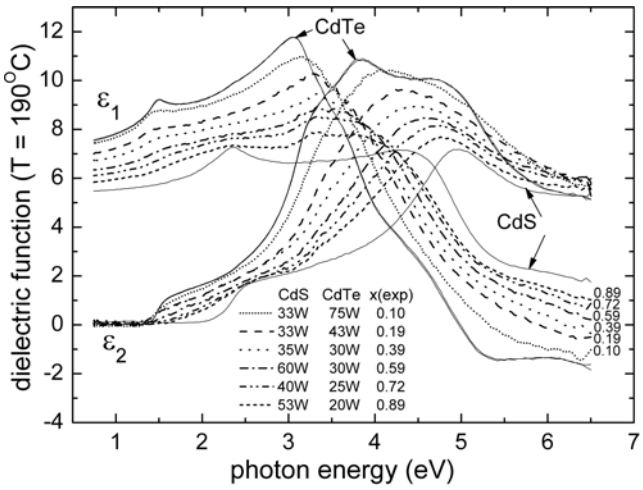


**Figure 7** Dielectric functions at the deposition temperature of $T = 190$ °C for $CdTe_{1-x}S_x$ alloy thin films prepared using different CdS and CdTe target RF powers to achieve different values of $x$.

### 3.3 $CdTe_{1-x}S_x$ films and CdS/CdTe interfaces

Growth rate calibrations of thin film CdS and CdTe have been undertaken in order to fabricate $CdTe_{1-x}S_x$ with controlled compositions by magnetron co-sputtering of CdTe and CdS targets. Figure 7 shows the $T = 190$ °C dielectric functions $\varepsilon$ of the resulting $CdTe_{1-x}S_x$ films deposited to thicknesses of 200–300 Å, as measured by RTSE. These $\varepsilon$ spectra are analyzed in order to compile a database that enables prediction of $\varepsilon$ for $CdTe_{1-x}S_x$ of any $x$ value. The database was applied in the analysis of RTSE results collected during $T = 190$ °C depositions of CdTe on CdS/c-Si, and the reverse sequence of CdS on CdTe/c-Si as shown in Fig. 8. In this study, a virtual interface approximation is applied to the RTSE data to find $x$ for the topmost ~8 Å of deposited material during interface formation. In both deposition sequences, there is a ~40 Å layer with a strong gradient in $x$, possibly generated by ion impact in the sputtering process. Beyond this thickness, S diffusion into CdTe exhibits a tail with $x \sim 0.02$; whereas for the inverted structure, Te diffusion into CdS exhibits a negligible tail, indicating a lower diffusion coefficient.

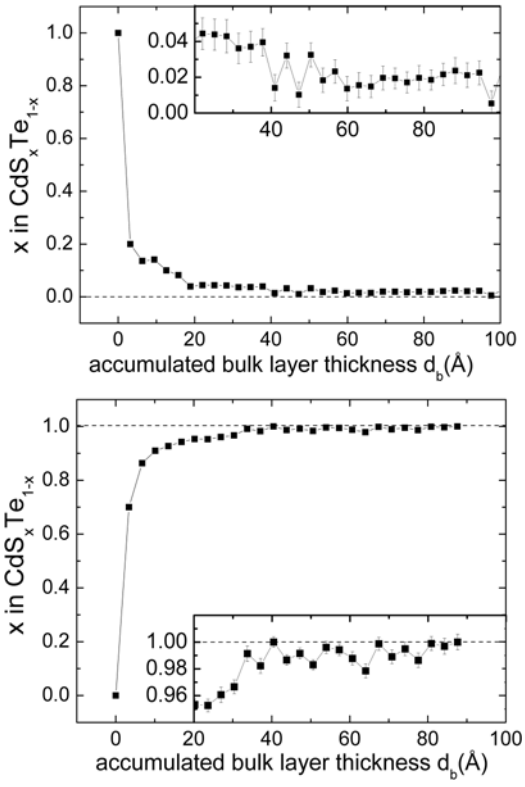


**Figure 8** Composition profiles $x(d_b)$ in $CdTe_{1-x}S_x$ for depositions at $T = 190$ °C for CdTe on CdS (upper) and CdS on CdTe (lower).

**4 Conclusion** RTSE has been applied to investigate the structural evolution and dielectric functions $\varepsilon$ of sputtered CdTe, CdS, and $CdTe_{1-x}S_x$ thin films. Key characteristics have been deduced including growth modes and final grain size. The database in $\varepsilon$ for $CdTe_{1-x}S_x$ enables analysis of inter-diffusion at CdS/CdTe and CdTe/CdS heterojunctions.

**Acknowledgements** The authors thank Prof. A. Compaan and his group at The University of Toledo. This study is supported by NREL under Subcontract No. RXL-5-44205-01.

## References

[1] A. Gupta and A. Compaan, Appl. Phys. Lett. **85**, 684 (2004).
[2] R. W. Collins, A. S. Ferlauto, G. M. Ferreira, C. Chen, J. Koh, R. J. Koval, Y. Lee, J. M. Pearce, and C. R. Wronski, Sol. Energy Mater. Sol. Cells **78**, 143 (2003).
[3] J. Li, J. Chen, J. Zapien, N. Podraza, C. Chen, J. Drayton, A. Vasko, A. Gupta, S. Wang, R.W. Collins, and A. Compaan, Mater. Res. Soc. Symp. Proc. **865**, F12.1 (2005).
[4] B. E. McCandless, G. M. Hanket, D. G. Jensen, and R. W. Birkmire, J. Vac. Sci. Technol. A **20**, 1462 (2002).
[5] J. Lee, P. I. Rovira, I. An, and R. W. Collins, Rev. Sci. Instrum. **69**, 1800 (1998).
[6] I. An, H. V. Nguyen, N. V. Nguyen, and R. W. Collins, Phys. Rev. Lett. **65**, 2274 (1990).
[7] J. A. Venables, G. D. T. Spiller, and M. Hanbucken, Rep. Prog. Phys. **47**, 399 (1984).
[8] J. Li, J. Chen, N. J. Podraza, and R. W. Collins, Proceedings of the 4th World Conference on Photovoltaic Energy Conversion (IEEE, Piscataway, NJ, 2006), p. 392.
[9] S. Ninomiya and S. Adachi, J. Appl. Phys. **78**, 1183 (1995).
[10] R. W. Collins and A. S. Ferlauto, in: Handbook of Ellipsometry, edited by H. G. Tompkins and E. A. Irene (William Andrew, Norwich, NY, 2005), p. 152.
[11] J. I. Pankove, Optical Processes in Semiconductors (Dover, New York, 1975).
[12] G. F. Feng and R. Zallen, Phys. Rev. B **40**, 1064 (1989).